Electronic Supplementary Material (ESI) for Journal of Materials Chemistry A.

A High-Throughput, Solvent Free Method for Dispersing Metal Atoms Directly onto Supports

Emerson C. Kohlrausch,[a,b] Higor Andrade Centurion,[c] Rhys W. Lodge,[a] Xuanli Luo,[d] Thomas Slater,[e] Marcos J. L. Santos,[b] Sanliang Ling,[d] Valmor R. Mastelaro,[c] Matthew Cliffe,[a] Renato Vitalino Goncalves[c] and Jesum Alves Fernandes[a*]

[a]School of Chemistry, University of Nottingham, Nottingham, NG7 2RD, UK.

[b]Programa de Pós-Graduação em Ciência dos Materiais, Universidade Federal do Rio Grande do Sul, 91501-970, Porto Alegre, RS, Brasil.

[c]São Carlos Institute of Physics, University of São Paulo, PO Box 369, 13560-970 São Carlos, SP, Brazil.

[d]Advanced Materials Research Group, Faculty of Engineering, University of Nottingham, Nottingham, NG7 2RD, UK.

[e]Electron Physical Sciences Imaging Centre, Diamond Light Source Ltd., Oxfordshire, OX11 0DE, UK.

1. Synthesis of graphitic carbon nitride (*g*-C_3N_4)

Bulk *g*-C_3N_4 was synthesised by heating 10 g of melamine powder in an alumina crucible at 300 °C for 2 h. The temperature was ramped to 520 °C for 2 h to produce the bulk *g*-C_3N_4 (Scheme S1).[1, 2]

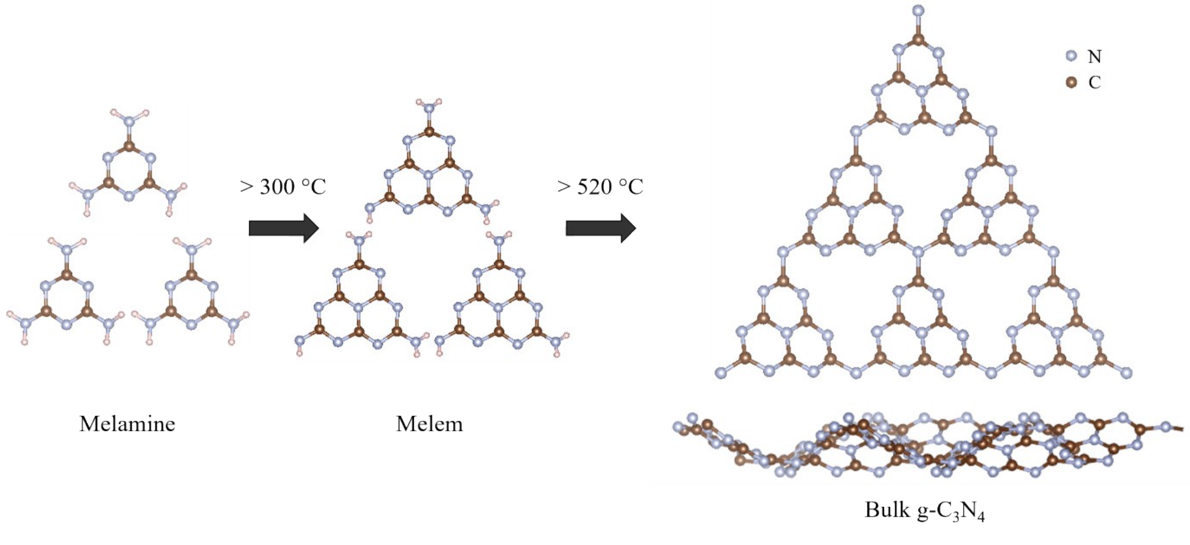

Scheme S1. Schematic illustration the synthesis of bulk *g*-C_3N_4.

2. Magnetron Sputtering Deposition

All depositions were carried out using a bespoke AJA magnetron sputtering system (Figure S1). *g*-C_3N_4 (1 g) was placed into a tailor-made stirring sample-holder, which stirred the *g*-C_3N_4 powder during the deposition process, and then loaded in the magnetron sputtering pre-chamber, reaching $3x10^{-7}$ Torr background pressure in 40 min. The sample-holder was transferred to the main chamber where the background-pressure was $3x10^{-8}$ Torr. After closing the gate-vale, and therefore isolating the main chamber from the pre-chamber, it took 10 min to stabilize the main chamber background-pressure back to $3x10^{-8}$ Torr. The Pt deposition was carried out with work-pressure of 3 mTorr using Ar gas, high purity Pt target (99.95%) under room temperature. The applied power utilized was 60 W (370 V and 16 mA) for 12 min.

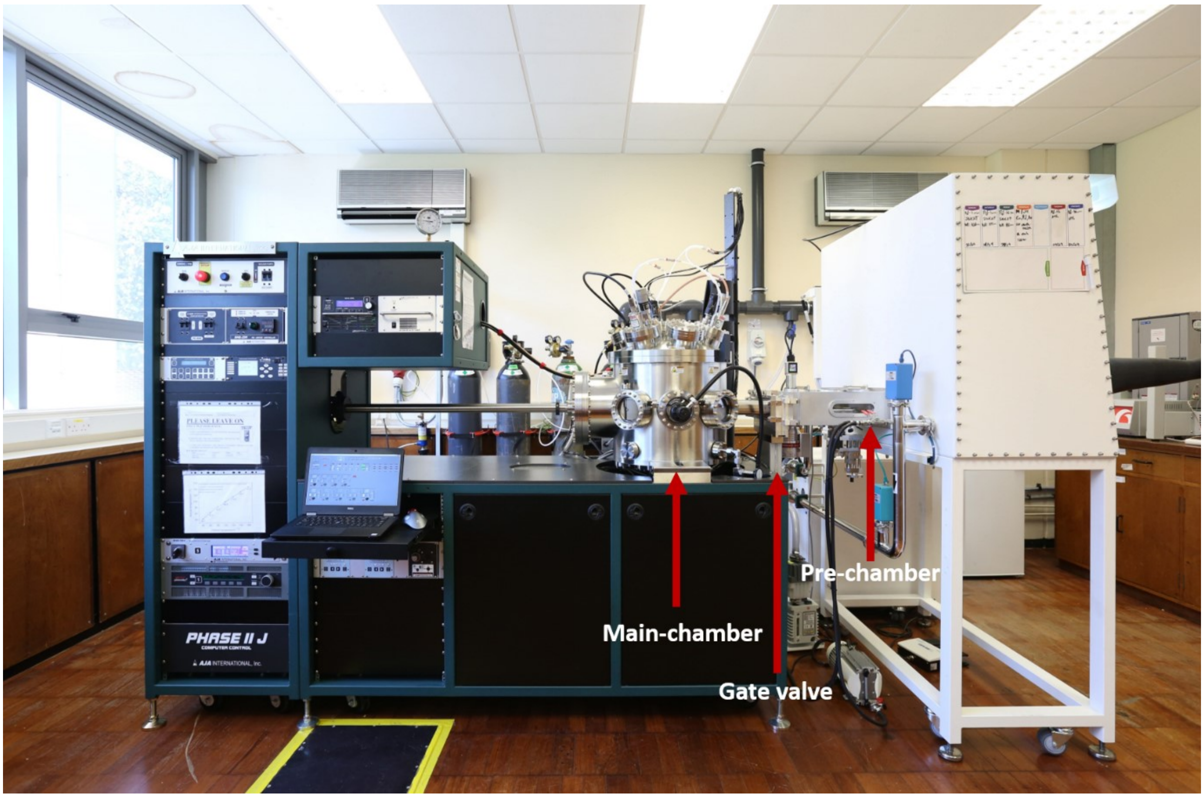

Figure S1. Magnetron sputtering system coupled to a glovebox, used in this work. For the metal deposition the samples were loaded and unloaded through the pre-chamber to the main-chamber, therefore the glovebox was not used in this work.

3. General characterisation

CHN Elemental analysis was carried out on a CHN Exeter Analytical CE-440 using helium (99.997% purity) as a carrier and oxygen for the combustion (99.995% purity). Infra-Red (IR) analyses were conducted using a Bruker Alpha (Fourier transform infrared) FTIR spectrometer with an ATR attachment. Data collection utilized 256 cumulative scans with a resolution of 4 cm^{-1}. N_2 isotherms of the catalysts, previously degassed at 180 °C under vacuum for 24 h, were obtained using TriStar and 3Flex Micromeritics instruments. Specific surface areas were determined by the BET multipoint method. Powder X-ray Diffraction (XRD) spectra were recorded using a voltage of 40 kV and current at 40 mA within range of $2\theta = 5° - 60°$ (Cu-Kα = 0.154 nm). To observe the single atoms in the samples, high-angle annular dark field (HAADF) STEM micrographs were obtained using a JEOL ARM200F microscope at the electron Physical Sciences Imaging Centre (ePSIC) at Diamond Light Source. An acceleration voltage of 200 kV was used throughout the measurements, with a beam current of approximately 15 pA, a convergence semi-angle of 23 mrad and a HAADF inner angle of 80 mrad. STEM samples were prepared by drop-casting a methanolic suspension of the sample onto a gold mesh, lacey carbon film TEM grid and allowing it to dry under ambient conditions. X-rays absorption (XAS) measurements were performed at room temperature at the Ni K-edge in the BL18 beamline at the Diamond Light Source and MAX-IV laboratory. X-ray absorption near edge structure (XANES) and Extended X-rays Absorption Fine Structure (EXAFS) spectra of the Pt/*g*-C_3N_4, Pt foil and PtO_2 standards were measured and the energy calibrated by aligning the respective absorption edges. The data were calibrated and normalized by a linear pre-edge subtraction using ATHENA software. The calculated Fourier transformed EXAFS spectra of these phases were obtained using ATHENA software. UV-Vis diffuse reflectance measurements were performed using a CARY 5000 spectrophotometer. Photoluminescence (PL) analyses were performed using a FLS1000 spectrometer from Edinburgh Instruments (excitation wavelength: 300 nm). X-ray photoelectron spectroscopy (XPS) measurements were performed using a Kratos AXIS Ultra DLD instrument. The chamber pressure during the measurements was $6.7 \times 10{-}7$ Pa. Wide energy range survey scans were collected at pass energy of 80 eV in hybrid slot lens mode and a step size of 0.5 eV, for 20 min. High-resolution data on the Pt 4f, C 1s and N 1s photoelectron peaks was collected at a pass energy of 20 eV over energy ranges suitable for each peak, and collection times of 5 min, step sizes of 0.1 eV. The charge neutraliser filament was used to prevent the sample charging over the irradiated area. The X-ray source was a monochromated Al Kα emission, run at 10 mA and 12 kV (120 W). The energy range for each 'pass energy' was calibrated using the Kratos Cu $2p_{3/2}$, Ag $3d_{5/2}$ and Au $4f_{7/2}$ three-point calibration method. The transmission function was calibrated using a clean gold sample method for all lens modes and the Kratos transmission generator software within Vision II. The data were processed with CASAXPS (Version 2.3.17). The high resolution data was charge corrected to the reference C 1s signal at 284.8 eV.

Table S1. CHN and specific surface area analysis of *g*-C_3N_4 and Pt/*g*-C_3N_4 did not show significant changes between the samples.

Sample	C %	N%	H %	N/C	Surface area (m^2/g)
g-C_3N_4	34.7	61.7	1.6	1.78	6.6
Pt/*g*-C_3N_4	34.7	61.7	1.6	1.78	6.3

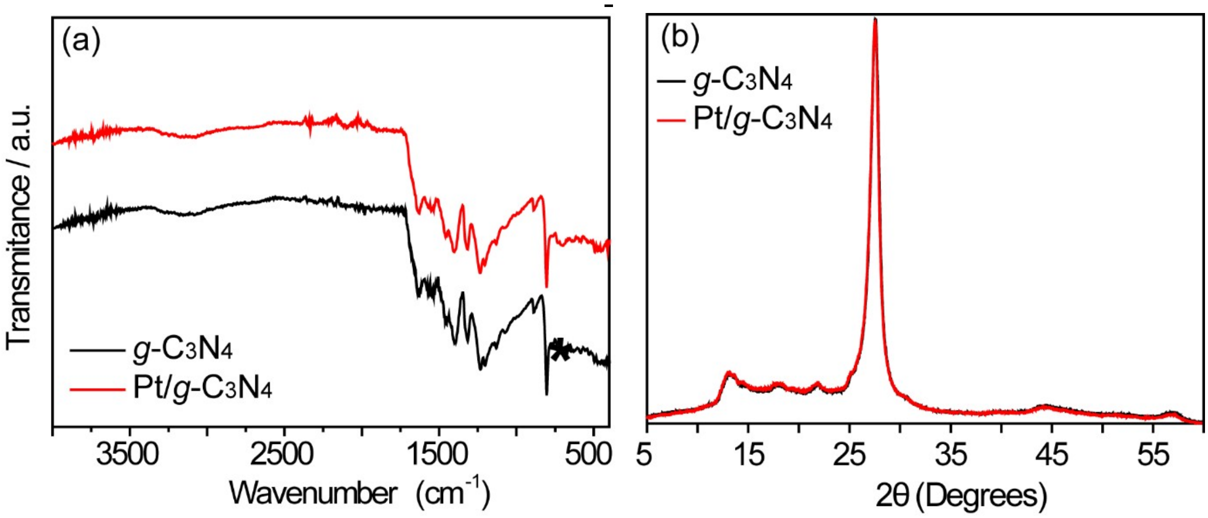

Figure S2. *g*-C_3N_4 and Pt/*g*-C_3N_4 measurements: **(a)** IR and **(b)** PXRD, 2θ ≈ 27°, corresponding to the (002) reflection of the interlayer stacking of aromatic segments d-spacing of 0.32 nm, 2θ ≈ 13°, corresponding to the in-plane (100) reflection with a d-spacing of 0.64 nm.

FTIR analysis showed the characteristic breathing mode of the triazine units at 801 cm^{-1} and strong bands in the 1200-1650 cm^{-1} region that corresponds to the typical stretching modes of C-N heterocycles (Figure S2a).[3, 4] PXRD analysis of the synthetized *g*-C_3N_4 showed the expected main diffraction peaks at 2θ ≈ 27°, corresponding to the (002) reflection of the interlayer stacking of aromatic segments d-spacing of 0.32 nm, and at 2θ ≈ 13°, corresponding to the in-plane (100) reflection with a d-spacing of 0.645 nm (Figure S2b).[3] These results therefore confirmed the synthesis of extended *g*-C_3N_4 networks.

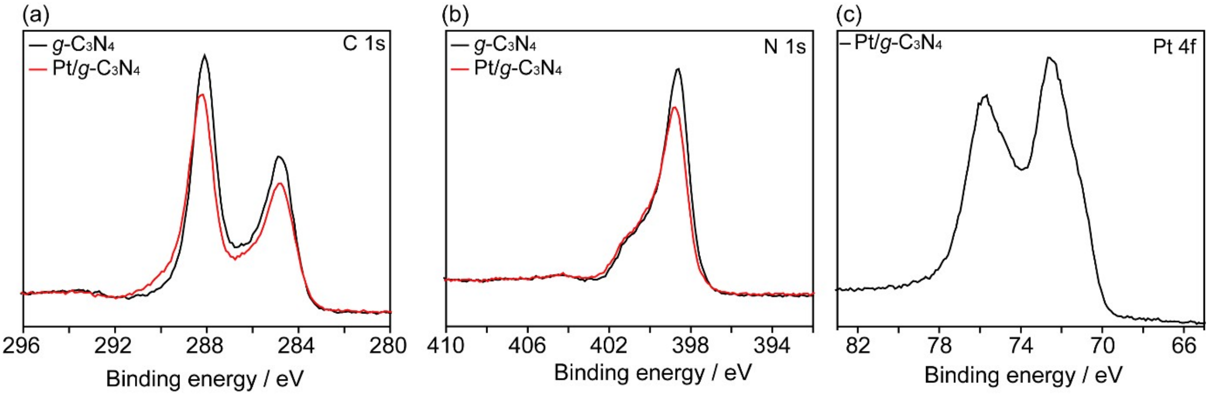

Figure S3. XPS analysis of *g*-C_3N_4 and Pt/*g*-C_3N_4: **(a)** C1s spectra shows a peak at *ca.* 288 eV which is ascribed to N-C=N group and another peak at *ca.* 285 eV associated to adventitious carbon.[3, 5] **(b)** N1s spectra show a main peak at *ca.* 398 eV of the two-coordinated (N_{2c}) nitrogen atoms, with a second component at *ca.* 400 eV associated to the three-coordinated (N_{3c}) nitrogen atoms and minor peak at *ca.* 404 eV which may be associated to positive charge localization in heterocycles due to π – excitations.[3, 5] **(c)** Pt $4f_{7/5}$ peak appears at *ca.* 73 eV showing a positive binding energy shift when compare with Pt^0 indicating the coordination of Pt-C/N bonds; which corroborates with XANES results.[6]

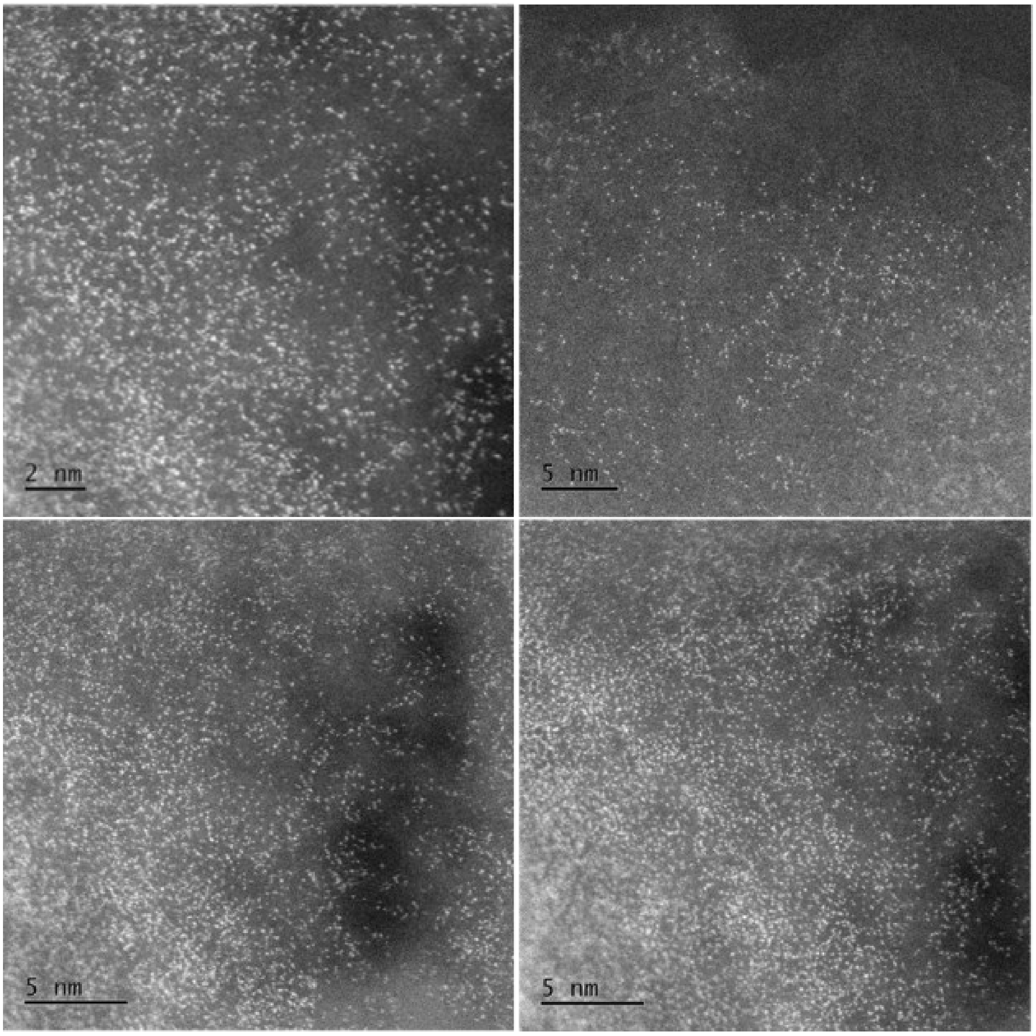

Figure S4. AC-STEM images of Pt/*g*-C_3N_4 showing the high dispersion of atomic platinum.

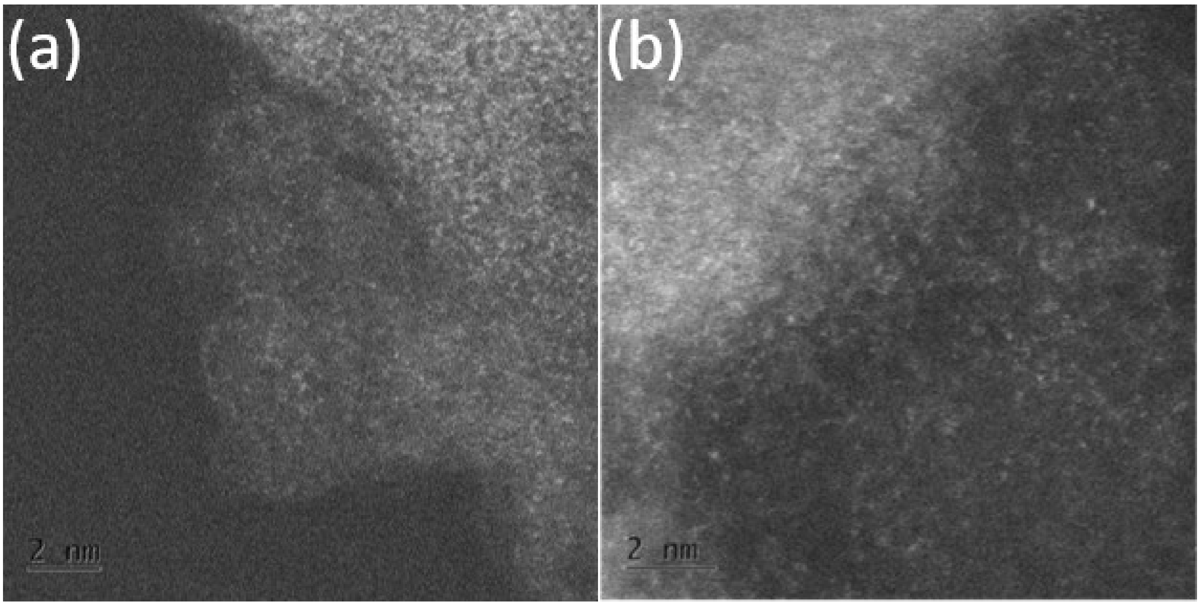

Figure S5. AC-STEM images of (**a, b**) Ni/*g*-C_3N_4 and Co/g-C_3N_4, respectively, showing the high dispersion of atomic nickel and cobalt. The magnetron sputtering depositions of Ni and Co atoms were carried out with work-pressure of 3 mTorr using Ar gas, high purity Ni and Co targets (99.95%) under room temperature. The applied power utilized was 20 W (283 V and 72 mA) for 60 min yielding Ni/*g*-C_3N_4 and Co/*g*-C_3N_4 0.5 wt% of Ni or Co onto 1 g of *g*-C_3N_4 ICP-OES.

Table S2. EXAFS experimental bond distances (not phase-corrected) for Pt foil, PtO_2 standard and Pt/*g*-C_3N_4.

Material	**Bond Type**	**Bond Distances (Å)**	
Pt - Foil	Pt-Pt	2.59	*This work*
PtO_2 - Standard	Pt-O	1.67	*This work*
	Pt-Pt	2.86-3.10	
Pt/*g*-C_3N_4	Pt-N/C	1.55	*This work*
	Pt-N/C	1.5	*Adv. Mater. 2016, 28, 2427–2431*
	Pt-N	1.67	*Nano Energy 2020, 69, 104409*
	Pt-N/C	1.61	*ACS Nano 2020, 14, 11394-11405*

4. Computational details

All density functional theory (DFT) calculations, including structural optimizations and total energy calculations, were performed using the Vienna Ab initio Simulation Package[7] with periodic boundary conditions. We used a plane-wave basis set with a kinetic energy cutoff of 400 eV to expand the wave functions. The Perdew-Burke-Ernzerhof functional[8] in combination with Grimme's D3 van der Waals correction[9] with the Becke-Johnson damping,[10] and the projector augmented wave method[11, 12] were used to solve the Kohn-Sham equations. A firstorder Methfessel-Paxton smearing[13] with a width of 0.2 eV was used to improve the convergence of electronic self-consistent field calculations. A monolayer of tri-s-triazine based *g*-C_3N_4 (see Figure 1) was considered in all DFT calculations. The vacuum gap between the periodic slabs was set to be ~15 Å. A Γ-centred Monkhorst-Pack *k*-point grid, with *k*-point spacing of ~0.10 Å^{-1}, was generated to sample the Brillouin zone. An energy convergence threshold of 10^{-4} eV was used for all total energy calculations, and the structural optimizations, including cell parameters and atomic positions, were considered converged if all interatomic forces fall below 0.01 eV/Å. We summarise relevant bonding distances taken from experimental literatures (for bulk Pt and PtO_2 references) and from our DFT calculations for different configurations of Pt/*g*-C_3N_4 (Table S3).

Table S3. Bond distances corresponding to the first/second coordination shell for Pt foil, PtO_2 standard and Pt/*g*-C_3N_4 are listed for some of our DFT optimized structures.

Material		**Bond Type**	**Bond Distances (Å)**
Pt - Foil		Pt-Pt	2.79
PtO_2 - Standard		Pt-O	1.92
		Pt-Pt	3.14
Pt/*g*-C_3N_4	Pt onto triazine based *g*-C_3N_4	Pt-N	1.90
		Pt-C	2.92
	Pt onto tri-s-triazine based *g*-C_3N_4	Pt-N	2.07
		Pt-C	2.73

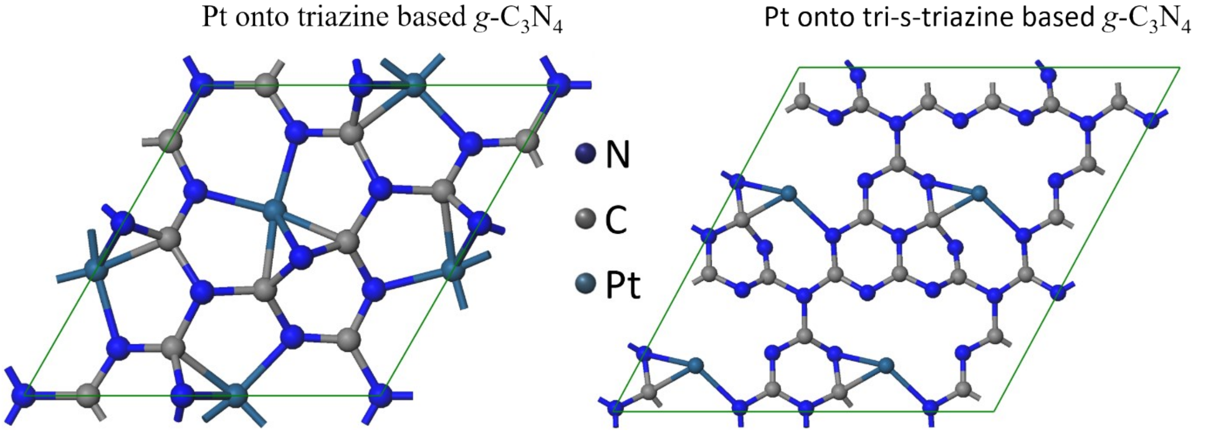

Figure S6. DFT optimized structures of Pt monomer stabilized by threefold nitrogen-interstice between s-triazine units and by a sixfold nitrogen-interstice between tri-s-triazine units in g-C_3N_4 framework.

5. Photocatalytic hydrogen evolution

The hydrogen evolution was performed using catalyst (50 mg) dispersed in an aqueous triethanolamine solution (50 mL, 10 vol%) in a 90 ml quartz reactor, linked by a gas line to a gas chromatograph (GC) (Agilent 7890B), with a thermal conductivity detector (TCD). Before the reaction, the suspension was sonicated for 30 min to obtain well dispersed particles. The system was purged with argon gas and vacuum 10 times to remove oxygen from the atmosphere. The quartz reactor was irradiated with a 300 W Xe Lamp (Cermax) using an AM1.5G filter and the infrared portion was excluded by a water filter. H_2 measurements were carried out at 1 h intervals. The irradiation intensity (300 mW.cm^{-2}) at the reactor was obtained using a photometer (Gentec XLP 12-3S-H2-D0).

Table S4. Photocatalytic measurements of g-C_3N_4 and Pt/g-C_3N_4.

Time / h	g-C_3N_4 (µmol)	Pt/g-C_3N_4 (µmol)
1	-	10.6998 ± 1.5023
2	-	32.1932 ± 1.6023
3	-	52.6595 ± 1.0265
4	0.0151 ± 0.0051	71.5924 ± 0.9654
5	0.0274 ± 0.0038	90.0344 ± 0.9236

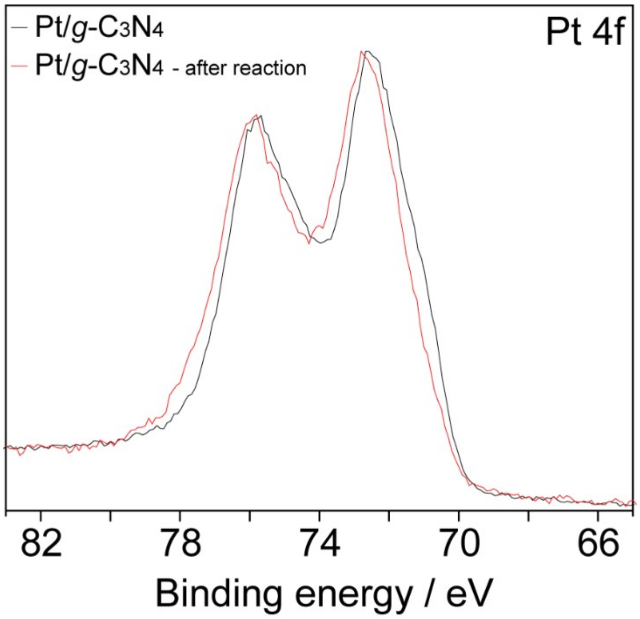

Figure S7. XPS measurements of Pt/g-C_3N_4[14] before and after reaction. Pt/g-C_3N_4 sample were filtered and then dried under reduced atmospheric before the XPS analysis.

Table S5. Summary of ADMCs preparation using different synthetic methods.

Synthetic Method	Metals	Support	Metal loading (wt%)	Chemicals	Temperature (°C)	Total time (h)	Metal production (mg h^{-1})	Reference
Magnetron sputtering	Pt	*g*-C_3N_4 (1 g)	0.5	Metal target, Argon	RT	1.03	4.8	*Our work*
Mechanochemical synthesis	Ni	N-carbon*	-	$C_4H_6NiO_4$. $C_{12}H_8N_2.H_2O$	400 - 700	18**	-	*Nano Energy 2021, 80, 105535*
Impregnation	Pt, Pd, Ru , Au	Activate carbon (1 g)	1	Metal precursors, solvents	61 to 66	16**	0.63	*Nat. Chem. 2020, 12, 560*
Impregnation, pyrolysis	Pt	Ceria NP*	4	K_2PtCl_4, H_2O, ethanol	850	28**	-	*Energy Environ. Sci. 2020,13, 4903*
pyrolysis	Ni	N-graphene (7.2 g)	-	$Ni(NO_3)_2.6H_2O$, water, ethanol, N_2	900	28**	-	*J. Mater. Chem. A 2020,8, 6190*
Pyrolysis	Fe	N-carbon (~30 mg)	3.46	SiO_2-PCN-222(Fe), HF	800	20**	0.052	*Nat Commun. 2020, 11, 2831*
Ion exchange	Pt	*g*-C_3N_4 (0.1 g)	10.8	$Pt(NH_3)_4Cl_2$, solvents	RT	36**	0.30	*Nano Energy 2020, 69, 104409*
Impregnation, pyrolysis	Fe	N-carbon (0.4 g)	1.05	$FeCl_3$, $(NH_4)_2S_2O_8$, HCl, N_2	900	86**	0.049	*Energy Environ. Sci. 2019, 12, 640*
Impregnation	Ni	N-graphene (0.1 g)	2.6	$NiCl_2$, NH_3	750	5**	0.52	*ACS Catal. 2018, 8, 11863*
MW irradiation	Pd	*g*-C_3N_4 (0.5 g)	1.25	$Pd(NH_3)_4(NO_3)_2$, water	-	14**	0.45	*Nat. Nanotech. 2018, 13, 702*
Liquid-phase	Pt	*g*-C_3N_4 (50 mg)	0.16	H_2PtCl_6, water, ethanol, Argon	60 to 125	9**	0.0089	*Adv. Mater. 2016, 28, 2427*
Photochemical route	Pd	TiO_2 (17.4 mg)	1.5	H_2PdCl_4, water	RT	8**	0.033	*Science 2016, 352, 797-800*

*Information not found.

** Parameters not accounted for the total time of synthesis of metal atoms: support material synthesis; heating ramp for pyrolysis/annealing process; reagents additions (including drop-wise); catalyst filtration and "washing", in some cases the mixture stirring time was not described (overnight experiments were considered for 12 hours).

Table S6. Photocatalytic hydrogen production.

Photocatalyst	Metal mean diameter size (nm) and loading (wt%)	Conc. (mg.ml^{-1})	Medium	T (ºC)	Irradiation (mW.cm^{-2}) / filter	Enhancing factor* (Metal-Support / Support)	Reference
Pt/*g*-C_3N_4	SAC / 0.3	1	H_2O + TEOA 10% vol	RT	300 / AM1.5G	3333.3	This work
Pt/*g*-C_3N_4	SAC / 0.16	0.25	H_2O + TEOA 10% vol	-	-	48.9	*Adv. Mater. 2016, 28, 2427*
Pt/*g*-C_3N_4	*c.a.* 5 / -	1	H_2O + TEOA 10% vol	-	- / >420 nm	1538.5	*Nano Energy 2016, 27, 138*
Pt/*g*-C_3N_4	SAC / 0.11	0.15	H_2O + CH_3OH 10% vol	10	100 / AM1.5G	21.1	*ACS Appl. Energy Mater. 2018, 1, 6082*
Pt-NCDs/TiO_2	SAC / -	-	0.3 M Na_2S and 0.3 M Na_2SO_3	-	500 / >420 nm	16.7	*J. Mater. Chem. A 2020, 8, 14690*
Pt/def-TiO_2	SAC / 0.99	0.5	H_2O + CH_3OH 10% vol	-	-	78.4	*Angew.Chem. 2020, 59,1295*
Ru/C_3N_4	Ru_6 / 0.01	2	H_2O + TEOA 15% vol	-	- / >420 nm	23.3	*ChemCatChem 2019, 11, 1963*

* The enhancing factor is how much the photocatalytic hydrogen production increased with the addition of metal co-catalyst in a support. This is calculated using hydrogen generation of metal/support divided by hydrogen generation by the pristine support (without metal co-catalyst).

6. References

1. Z. Mo, X. She, Y. Li, L. Liu, L. Huang, Z. Chen, Q. Zhang, H. Xu and H. Li, *RSC Advances*, 2015, **5**, 101552-101562.
2. M. Ismael and Y. Wu, *Sustainable Energy & Fuels*, 2019, DOI: 10.1039/C9SE00422J.
3. I. Papailias, T. Giannakopoulou, N. Todorova, D. Demotikali, T. Vaimakis and C. Trapalis, *Applied Surface Science*, 2015, **358**, 278-286.
4. P. Sharma and Y. Sasson, *Green Chemistry*, 2017, **19**, 844-852.
5. J. Fang, H. Fan, M. Li and C. Long, *Journal of Materials Chemistry A*, 2015, **3**, 13819-13826.
6. H. Zhang, P. An, W. Zhou, Y. Guan Bu, P. Zhang, J. Dong and W. Lou Xiong, *Science Advances*, **4**, eaao6657.
7. G. Kresse and J. Furthmüller, *Physical Review B*, 1996, **54**, 11169-11186.
8. J. P. Perdew, K. Burke and M. Ernzerhof, *Physical Review Letters*, 1996, **77**, 3865-3868.
9. S. Grimme, J. Antony, S. Ehrlich and H. Krieg, *The Journal of Chemical Physics*, 2010, **132**, 154104.
10. S. Grimme, S. Ehrlich and L. Goerigk, *Journal of Computational Chemistry*, 2011, **32**, 1456-1465.
11. P. E. Blöchl, *Physical Review B*, 1994, **50**, 17953-17979.
12. D. Hobbs, G. Kresse and J. Hafner, *Physical Review B*, 2000, **62**, 11556-11570.
13. M. Methfessel and A. T. Paxton, *Physical Review B*, 1989, **40**, 3616-3621.
14. Y. Cao, D. Wang, Y. Lin, W. Liu, L. Cao, X. Liu, W. Zhang, X. Mou, S. Fang, X. Shen and T. Yao, *ACS Applied Energy Materials*, 2018, **1**, 6082-6088.